This article has been accepted for inclusion in a future issue of this journal. Content is final as presented, with the exception of pagination.

Prediction of CO_2 Saturation Spatial Distribution Using Geostatistical Inversion of Time-Lapse Geophysical Data

Dario Grana, Mingliang Liu, and Mohit Ayani

***Abstract*— Carbon dioxide sequestration in deep saline aquifers and depleted reservoirs relies on numerical models for the prediction of the spatial distribution of CO_2 saturation during injection and migration. Due to the limited knowledge of the rock and fluid properties before injection, model predictions are often uncertain and must be updated when new measurements are available. The spatial distribution of CO_2 saturation and the plume location can be monitored using time-lapse geophysical data, such as seismic and controlled source electromagnetic surveys. We propose a geostatistical inversion approach for the prediction of the time-dependent spatial distribution of CO_2 saturation from geophysical data. The methodology is based on the application of a stochastic optimization method, the Ensemble Smoother, for the solution of the inverse problem, using rock physics and geophysical models. The inversion is applied to the difference in the geophysical data acquired before and during injection. The predicted models of CO_2 saturation are obtained by updating an ensemble of geostatistically generated prior realizations, based on the misfit between geophysical model predictions and measured data. The novelty of the approach is the integration of geostatistical algorithms and stochastic optimization methods for the joint inversion of geophysical data. The proposed approach allows including hydrological constraints in the prior model and quantifying the prediction uncertainty due to the noise and resolution of the data and approximations in the physical relations. The method is applied to the Johansen formation model, offshore Norway, using synthetic seismic and electromagnetic data.**

***Index Terms*— CO_2 sequestration, inverse problems, reservoir geophysics, rock physics, stochastic methods.**

I. Introduction

MONITORING of injection and migration of CO_2 in deep saline aquifers requires accurate and precise predictions of the temporal–spatial distribution of CO_2 and water, that is, the saturation values of CO_2 and water at each location in the reservoir and their changes through time [1]. If the distributions of CO_2 and water are known at a given time during injection or migration, their distribution at any future time can be predicted by simulating the fluid flow in the aquifer, according to the injection parameters and the petrophysical properties of the porous rocks, such as porosity and permeability. Fluid flow models and stochastic simulations are commonly used in geoscience applications to predict fluid displacement in porous rocks, as in hydrogeology [2] and energy resources [3]. However, the rock and fluid properties in the subsurface are generally unknown due to the lack of direct measurements that are generally available at the borehole locations only. Therefore, the predictions of fluid saturations are generally uncertain and often inaccurate. The rock and fluid properties can be predicted and updated using the available geophysical data (seismic, electromagnetic, or gravity data) by solving inverse problems based on geophysical models, such as rock physics, seismic wave propagation, and electromagnetic equations [4].

Carbon capture, utilization, and storage in deep saline aquifers have been widely studied [1], [5], and [6]. Several studies focus on geological and geophysical methods to quantify the capacity of the storage unit and fluid flow simulation to predict the CO_2 plume location and the pressure front extent [7]–[12]. Geophysical surveys, in particular reflection seismic data, have often been used for pre-injection reservoir characterization [13]–[20]. Most of these studies use seismic data to predict the petrophysical properties, primarily porosity. Controlled source electromagnetic data are generally more sensitive to fluid volumes than seismic data and are commonly used to map fluid saturations in the subsurface [21]–[30]. The joint inversion of seismic and electromagnetic data has been proposed in the recent geophysical literature [31]–[37]. However, a comprehensive workflow for updating saturation models and for uncertainty quantification based on fluid flow simulations and monitoring geophysical data is still missing.

The estimation of CO_2 and water saturation based on geophysical measurements during injection and migration is an inverse problem where the model variables are the time-dependent saturations in the reservoir and the data are the time-lapse geophysical measurements (i.e., seismic and electromagnetic responses). The goal is to predict the saturation values at any time and location in the reservoir and quantify their uncertainty. Several mathematical algorithms have been presented, including stochastic methods [17], [38], and [39]. In time-dependent problems, such as subsurface model updating with time-dependent data, data assimilation methods are

Manuscript received June 21, 2020; revised July 29, 2020; accepted August 20, 2020. *(Corresponding author: Dario Grana.)*

Dario Grana is with the Department of Geology and Geophysics, School of Energy Resources, University of Wyoming, Laramie, WY 82071 USA (e-mail: dgrana@uwyo.edu).

Mingliang Liu and Mohit Ayani are with the Department of Geology and Geophysics, University of Wyoming, Laramie, WY 82071 USA.

Color versions of one or more of the figures in this article are available online at http://ieeexplore.ieee.org.

Digital Object Identifier 10.1109/TGRS.2020.3018910

generally used to update the reservoir model. The ensemble-based methods represent a particular category of algorithms in which an ensemble of models is simultaneously updated to match the observed measurements. The ensemble-based methods include filtering and smoothing algorithms such as Ensemble Kalman filter and the Ensemble Smoother [40]–[43] and have been applied to borehole measurements and geophysical data [44]–[50].

In this work, we propose to apply the ensemble-based methods to fluid saturation predictions from time-lapse geophysical data. The proposed inversion approach combines geostatistical methods for the generation of the prior models and a stochastic optimization algorithm for the updating of the models conditioned on the geophysical data. To generate initial model realizations that preserve the hydrological realism of the saturation distributions, we propose to generate the prior realizations by sampling from a large ensemble of fluid flow simulations with variable petrophysical properties, and we update them based on the data misfit. The method is validated on the Johansen formation, offshore Norway. The reservoir model has been presented in [14] and [15]. The synthetic time-lapse geophysical data set includes seismic and controlled source electromagnetic (CSEM) data. The geostatistical approach to geophysical inversion allows predicting accurately the CO_2 and water spatial distributions, and the use of fluid flow simulations for prior models guarantees realistic hydrological features. We first predict the porosity from seismic data (pre-injection survey) assuming that the aquifer is initially saturated with water and then estimate the CO_2 saturation from time-lapse measurements. This study proves the value of the proposed probabilistic modeling method for monitoring the CO_2 plume displacement using geophysical data.

II. Methodology

We present the inversion method for the prediction of rock and fluid properties given a set of geophysical measurements.

A. Problem Setting

In the proposed mathematical notation, the model vector $\boldsymbol{m}$ represents the rock and fluid properties (porosity and CO_2 saturation) at each location in the spatial model at a given time and the data vector $\boldsymbol{d}$ represents the geophysical measurements, including seismic amplitudes and travel times and electromagnetic amplitudes and phases. The mathematical-physical operator $\boldsymbol{f}$ that links the model variables to the data predictions is given by

$$\boldsymbol{d} = \boldsymbol{f}(\boldsymbol{m}) + \boldsymbol{e} \tag{1}$$

where $\boldsymbol{e}$ is the error vector [51]. The operator $\boldsymbol{f}$ might include wave propagation equations, Maxwell's equations for the electrical and magnetic fields, and rock physics models to relate porosity and fluid saturations to electrical resistivity and elastic properties. The operator $\boldsymbol{f}$ might assume different formulations in different lithologies and rock formations depending on the mineral composition and structure of the porous rocks [4].

The solution of the inverse problem is an approximate model $\hat{\boldsymbol{m}}$ that minimizes the mismatch between data and model predictions

$$\hat{\boldsymbol{m}} = \mathrm{argmin}_{\boldsymbol{m}} ||\boldsymbol{d} - \boldsymbol{f}(\boldsymbol{m})||. \tag{2}$$

We adopt a Bayesian approach and compute the posterior distribution $p(\boldsymbol{m}|\boldsymbol{d})$ of the model parameters given the data using Bayes' rule

$$p(\boldsymbol{m}|\boldsymbol{d}) = kp(\boldsymbol{d}|\boldsymbol{m})p(\boldsymbol{m}) \tag{3}$$

where $p(\boldsymbol{m})$ is the prior distribution of the model parameters, $p(\boldsymbol{d}|\boldsymbol{m})$ is the likelihood associated with the operator $\boldsymbol{f}$, and $k = 1/p(\boldsymbol{d}) = 1/\int p(\boldsymbol{d}|\boldsymbol{m})p(\boldsymbol{m})d\boldsymbol{m}$ is a normalizing constant. In the proposed approach, the error vector $\boldsymbol{e}$ is assumed to be distributed according to a multivariate Gaussian distribution $N(\boldsymbol{e}; \boldsymbol{0}, \boldsymbol{\Sigma_e})$ with $\boldsymbol{0}$ mean and known covariance matrix $\boldsymbol{\Sigma_e}$ and is assumed independent of the model variables. The posterior mean of the distribution $p(\boldsymbol{m}|\boldsymbol{d})$ is the most probable model $\hat{\boldsymbol{m}}$ of porosity and CO_2 saturation.

B. Geophysical Forward Model

We first present the geophysical models used to predict the geophysical response of the aquifer model. The geophysical relations used to predict the seismic and electromagnetic response for all the possible combinations of rock and fluid properties in the model include the following: 1) elastic rock physics model; 2) electrical rock physics model; 3) seismic model; and 4) electromagnetic model.

We assume one mineral phase (e.g, quartz) and two fluid components, water and CO_2. Therefore, the variables of interest are porosity ϕ, water saturation S_w, and CO_2 saturation $1 - S_w$ (where the scalar notation is used to indicate the value at a given location in the model). There are several rock physics models to compute the elastic response (i.e., P-wave velocity, S-wave velocity, and density) of fluid saturated porous rocks with given porosity ϕ and water saturation S_w [4]. In the proposed approach, we use the soft sand model combined with Gassmann's equations and the density equation. The density of the fluid saturated rock $\rho(\phi, S_w)$ is computed as a multilinear function of porosity and water saturation

$$\begin{aligned}\rho(\phi, S_w) &= (1-\phi)\rho_m + \phi\rho_f = \\ &= (1-\phi)\rho_m + \phi[(1-S_w)\rho_{CO2} + S_w\rho_w]\end{aligned} \tag{4}$$

where ρ_m is the density of the mineral phase, and ρ_f is the density of the fluid mixture and depends on water saturation S_w and the densities of CO_2 and water, ρ_{CO2} and ρ_w. The P- and S-wave velocities are computed from the elastic moduli and density of the saturated rock. Because we assume one mineral phase, the bulk and shear moduli of the solid are the characteristic values of quartz [4]. In a multimineral setting, approximations of the elastic moduli can be computed using Voigt–Reuss–Hill or Hashin–Shtrikman elastic bounds [4]. The bulk and shear moduli of the dry rock, K_{ϕ_c} and G_{ϕ_c}, at the critical porosity ϕ_c (i.e., the maximum porosity of a porous rock, beyond which the system can be considered a suspension) are computed using Hertz–Mindlin equations

$$K_{\phi_c} = \sqrt[3]{\frac{c^2(1-\phi_c)^2 G_0^2}{18\pi^2(1-\nu_0)^2} P}$$
$$G_{\phi_c} = \frac{5-4\nu_0}{5(2-\nu_0)} \sqrt[3]{\frac{3c^2(1-\phi_c)^2 G_0^2}{2\pi^2(1-\nu_0)^2} P} \quad (5)$$

where c is the average number of contacts per grain, G_0 is the shear modulus of the solid phase (at 0 porosity), ν_0 is the Poisson's ratio of the solid phase, and P is the effective pressure. The bulk and shear moduli of the dry rock, $K_d(\phi) = k_{HS^-}(\phi, K_0, K_{\phi_c})$ and $G_d(\phi) = g_{HS^-}(\phi, G_0, G_{\phi_c})$, for porosity $\phi \in [0, \phi_c]$, are computed using an harmonic average of the elastic moduli of the solid phase (K_0, G_0) and the elastic moduli at the critical porosity (K_{ϕ_c}, G_{ϕ_c}), using the functions k_{HS^-} and g_{HS^-} representing the modified Hashin–Shtrikman lower bounds [4]. The bulk modulus of the saturated rock, $K_s(\phi, S_w)$ is computed using Gassmann's equation

$$K_s(\phi, S_w) = K_d(\phi) + \frac{\left(1 - \frac{K_d(\phi)}{K_0}\right)^2}{\frac{\phi}{K_f(S_w)} + \frac{(1-\phi)}{K_0} - \frac{K_d(\phi)}{K_0^2}} \quad (6)$$

where the bulk modulus of the fluid $K_f(S_w)$ is computed using Reuss average as

$$K_f(S_w) = \left(\frac{(1-S_w)}{K_{\mathrm{CO2}}} + \frac{S_w}{K_w}\right)^{-1} \quad (7)$$

with K_{CO2} and K_w being the bulk moduli of CO_2 and water, respectively, whereas the shear modulus of the saturated rock, $G_s(\phi, S_w)$, is equal to the shear modulus of the dry rock $G_d(\phi)$, according to Gassmann's theory [4]. The P- and S-wave velocities, V_P and V_S, are then computed as

$$V_P = \sqrt{\frac{K_s(\phi, S_w) + 4/3 G_s(\phi, S_w)}{\rho(\phi, S_w)}}$$
$$V_S = \sqrt{\frac{G_s(\phi, S_w)}{\rho(\phi, S_w)}} \quad (8)$$

where $\rho(\phi, S_w)$ is given by (4).

The resistivity R of the saturated rock can be calculated using Archie's law [4]

$$R = \frac{R_w}{\phi^m S_w^n} \quad (9)$$

where R_w is the resistivity of water, m is the cementation exponent, and n is the saturation exponent. These parameters are assumed to be constant. Archie's law is generally assumed to be valid in sandstone. Other rock physics models such as elastic inclusion models for elastic properties and electrical models accounting for clay inner resistivity [4] could also be applied.

The seismic response can be predicted by solving the poro-elastic wave equation. However, approximated models are also available. In this work, we adopt a convolutional model. Given a sequence of rock formations, their seismogram $\boldsymbol{s}(\theta)$ can be computed, for any reflection angle θ, as a function of the vectors of the P- and S-wave velocities and density, along the vertical profile. For weak elastic contrasts and small reflection angles, the seismic response $\boldsymbol{s}(\theta)$ can be accurately approximated as a convolution of the seismic wavelet $\boldsymbol{w}(\theta)$ and the P–P reflection coefficient series $\boldsymbol{r}(\theta)$ that depend on the P- and S-wave velocities $\boldsymbol{V_P}$ and $\boldsymbol{V_S}$, and density $\boldsymbol{\rho}$, according to Shuey's linearized approximation of Zoeppritz equations [52]. At a given travel time t, the corresponding seismic amplitude is given by

$$s(t,\theta) = w(t,\theta) * r(t,\theta) = \int w(t,\theta) r(t-u,\theta) du \quad (10)$$

where $*$ represents the convolution operator.

The CSEM electric field $\mathbf{E}$ and the magnetic field $\mathbf{H}$ can be computed based on the electrical resistivity obtained from Archie's law. The relations linking electrical conductivity $\sigma = 1/R$ (i.e., the reciprocal of resistivity) to the curl of the electric field $\mathbf{E}$ and curl of the magnetic field $\mathbf{H}$ are described by Maxwell's equations

$$\nabla \times \mathbf{E} - \mathrm{i}\omega\mu\mathbf{H} = \mathbf{M^S}$$
$$\nabla \times \mathbf{H} - \sigma\mathbf{E} = \mathbf{J^S} \quad (11)$$

where ω is the angular frequency, μ is the magnetic permeability (i.e. the resistance to the magnetic field), and $\mathbf{M^S}$ and $\mathbf{J^S}$ are the electric and magnetic sources, respectively. Assuming an isotropic 2-D conductivity model along the strike direction, Maxwell's equations can be solved using finite element methods in the frequency domain, as shown in [25] and [53]. The electrical conductivity, in principle, is complex and depends on the real electrical conductivity and the dielectric permittivity; however, for low-frequency sources, the conductivity is assumed to be equal to the real component. The 2-D formulation is extended to 3-D applications by applying Maxwell's equations section by section, where each section is processed independently.

In our approach, the reservoir properties, including porosity and fluid saturations, are defined in the irregular stratigraphic grid of the structural model and then interpolated on a regular grid for the calculation of the seismic data and on an adaptive triangular mesh for the calculation of the electromagnetic data. The spatial interpolation is considered part of the forward operator $\boldsymbol{f}$ in (1).

C. Inverse Method

Next, we introduce the inverse method. The inversion is divided in two steps: first, we predict porosity from the base seismic survey and, then, we predict CO_2 saturation from time-lapse seismic and electromagnetic data. The inverse method is based on the Ensemble Smoother [40], in which an ensemble of prior realizations is first generated and then updated using a Bayesian updating step based on the Kalman filter equations. We first discuss the prior model generation and then present the updating approach.

1) Prior Ensemble Generation: Prior model realizations of porosity and saturation can be generated using geostatistical simulations, such as Sequential Gaussian Simulations or Probability Field Simulations algorithms; however, saturation distributions are generally non-stationary due to the effects of gravity. Traditional algorithms might lead to unphysical model realizations that do not preserve the physical order of fluids or do not obey to hydrological constraints. In the proposed approach, we generate prior realizations according to two different approaches for porosity and saturations, respectively. For the prediction of porosity from the base seismic survey, we assume that the prior model of porosity is a truncated Gaussian random field with locally variable mean and known spatial covariance matrix. We then generate N_e prior realizations using the fast Fourier transform moving average (FFT-MA) method [54]. The FFT-MA generates a spatially correlated realization by computing the inverse Fourier transform of the product of the Fourier transform of a spatial filter (associated with the spatial covariance function) and the Fourier transform of a spatially uncorrelated realization of a standard Gaussian random field [54]. The FFT-MA method is extremely efficient to generate unconditional realizations; however, any other geostatistical algorithm could be used. For the prediction of CO_2 saturation from time-lapse data, we first generate N_e prior realizations of porosity and permeability, using the FFT-MA method, and then, for each realization, we run a fluid flow simulation and choose a saturation model at a random time according to a uniform distribution in the simulation time interval. It is possible to choose the saturation realizations at the time at which the data are measured, with the differences in the realizations being due to the initial porosity and permeability values; however, the variability of such ensemble is limited and the inversion might lead to an underestimation of the posterior uncertainty. Instead, the proposed approach generates a prior ensemble of saturation models with a large variability. The fluid flow simulation is conducted using MATLAB reservoir simulation toolbox (MRST) [55], specifically the MRST-co2lab tool, to mimic CO_2 and water displacement during injection and migration. We store the prior model realizations in the ensemble of vectors $\{\boldsymbol{m}_j^{\text{prior}}\}_{j=1,\dots,N_e}$.

Because volumetric fractions are bounded variables in the interval [0,1], we first apply a logit transformation to the model parameters to map porosity and saturations to the (unbounded) set of real numbers, then apply the inversion in the transformed space, and apply the inverse transformation to obtain the final predictions in the porosity and saturation bounded domain.

2) Ensemble Updating: The prior realizations are then updated using the Ensemble Smoother approach, where the covariance matrices are approximated using the sample covariance matrices estimated from the ensemble. The initial ensemble includes N_e models $\boldsymbol{m}_j$ for $j = 1, \dots, N_e$. The inversion approach can be summarized as follows.

1) For each model in the ensemble, we apply the geophysical functions in (4)–(11) to compute the corresponding seismic and electromagnetic response and we obtain the vector of the predicted data $\{\boldsymbol{d}_j^{\text{prior}}\}_{j=1,\dots,N_e}$
$$\boldsymbol{d}_j^{\text{prior}} = \boldsymbol{f}\left(\boldsymbol{m}_j^{\text{prior}}\right) + \boldsymbol{e}_j \tag{12}$$
where $\{\boldsymbol{e}_j\}_{j=1,\dots,N_e}$ represent the data errors.
2) For each model in the ensemble, we compute a stochastic perturbation $\{\boldsymbol{d}_{\boldsymbol{p}\,j}\}_{j=1,\dots,N_e}$ of the measured data $\boldsymbol{d}$ as
$$\boldsymbol{d}_{\boldsymbol{p}\,j} = \boldsymbol{d} + \boldsymbol{\Sigma}_{\boldsymbol{e}}^{1/2}\boldsymbol{z}_j \tag{13}$$
where $\boldsymbol{z}_j \sim N(\boldsymbol{0}, \boldsymbol{I}_n)$ is a vector sampled from a n-variate Gaussian distribution with $\boldsymbol{0}$ mean and covariance matrix equal to the $n \times n$ identity matrix $\boldsymbol{I}_n$, for $j = 1, \dots, N_e$, and $\boldsymbol{\Sigma}_{\boldsymbol{e}}^{1/2}$ is the square root of the covariance matrix of the measurement errors.
3) We then update the ensemble using the Ensemble Smoother updating equation [40]
$$\boldsymbol{m}_j^{\text{post}} = \boldsymbol{m}_j^{\text{prior}} + \boldsymbol{\Sigma}_{\boldsymbol{m},\boldsymbol{d}}^{\text{prior}}\left(\boldsymbol{\Sigma}_{\boldsymbol{d},\boldsymbol{d}}^{\text{prior}} + \boldsymbol{\Sigma}_{\boldsymbol{e}}\right)^{-1}\left(\boldsymbol{d}_{\boldsymbol{p}\,j} - \boldsymbol{d}_j^{\text{prior}}\right) \tag{14}$$
for $j = 1, \dots, N_e$ and obtain the ensemble of posterior models $\{\boldsymbol{m}_j^{\text{post}}\}_{j=1,\dots,N_e}$. In (14), the matrix $\boldsymbol{\Sigma}_{\boldsymbol{m},\boldsymbol{d}}^{\text{prior}}$ is the cross-covariance matrix of $\boldsymbol{m}^{\text{prior}}$ and $\boldsymbol{d}^{\text{prior}}$ and the matrix $\boldsymbol{\Sigma}_{\boldsymbol{d},\boldsymbol{d}}^{\text{prior}}$ is the covariance matrix of the data $\boldsymbol{d}^{\text{prior}}$.

In the ES-MDA [42], steps 1–3 are repeated to assimilate the measured data multiple times and improve the accuracy of the updated predictions, using inflation factors for the covariance matrix of the data errors. In the ensemble-based methods, it is also possible to update the model variables and the data predictions simultaneously; however, in the proposed implementation, we apply the updating to the model variables only [56] and compute the predicted data using the forward model. A sensitivity analysis on the covariance matrix of the error measurement $\boldsymbol{\Sigma}_{\boldsymbol{e}}$ is necessary. In our work, $\boldsymbol{\Sigma}_{\boldsymbol{e}}$ is assumed to be diagonal, but especially with real time-lapse geophysical data with imperfect repeatability, error correlations should be introduced to model processing errors in the data.

The inversion for porosity and time-dependent saturation can be solved sequentially or jointly. If we assume that before injection, there is only one fluid component (water) in the aquifer, and the base seismic survey is not affected by the fluid; therefore, the porosity model can be predicted from the preinjection seismic survey using the inverse method in (12)–(14), where the model vector $\boldsymbol{m}$ includes porosity and the data vector $\boldsymbol{d}$ includes the base seismic survey [49]. Then, fluid saturations are predicted from time-lapse geophysical data using the same inverse method, where the model vector $\boldsymbol{m}$ includes CO_2 saturation and the data vector $\boldsymbol{d}$ includes the difference in base and monitor seismic and electromagnetic surveys.

Because of the large dimension of geophysical data, the Ensemble Smoother approach is often not practical, since it would require a large number of initial realizations to obtain accurate predictions and a reliable quantification of uncertainty. To overcome this problem, we propose to apply a dimensionality reduction method to map the data in a smaller dimensional space and perform the inversion using the Ensemble Smoother in the reduced space [57]. The data reduction can be obtained using traditional methods such as principal component analysis or multidimensional scaling, or using deep learning algorithms, for example, the deep convolutional auto-encoder (DCAE). Deep learning methods

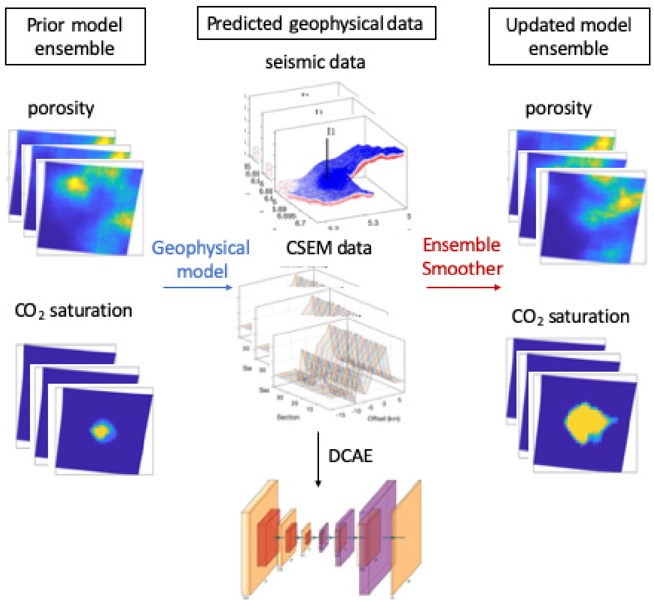

Fig. 1. Schematic of the inversion methodology.

have been successfully applied to seismic inversion [58] and [59]. In the proposed approach, we choose the DCAE approach to compress the data and preserve the spatial correlation structure [57]. The proposed method is schematically depicted in Fig. 1.

III. Application

We apply the proposed approach to a carbon dioxide sequestration study based on the Johansen formation model, offshore Norway. The Johansen formation is located below the Troll hydrocarbon field where existing boreholes are available. The data set has been presented in several publications including [14] and [15]. The data show favorable geological features of the storage unit and the overlying sealing, including pore volume, storage capacity, and pressure conditions. The formation depths are between 2200 and 3200 m.

A. Synthetic Data Generation

The pre-injection stratigraphic model of the Johansen formation was built based on seismic and well log data. A structural model including porosity and permeability spatial distributions is available [15]. The original geo-cellular model is discretized in 100 × 100 × 5 cells; however, in this study, we consider a smaller sub-volume of size 40 × 40 × 5 cells centered around the injection well (Fig. 2). The model includes a major fault interpreted from seismic data. The true reservoir model of porosity and permeability shows relatively high values in the top layers and lower values in the bottom layers. The initial water saturation (before injection) is equal to 1 everywhere. The fluid flow is simulated using MRST-co2lab with an injection period of 100 years and a constant injection rate of 1.4×10^4 m^3/day and migration time of 400 years. Synthetic seismic and CSEM data are computed before injection (base survey) based on the model in Fig. 2 and 10 years after stopping CO_2 injection (monitor survey)

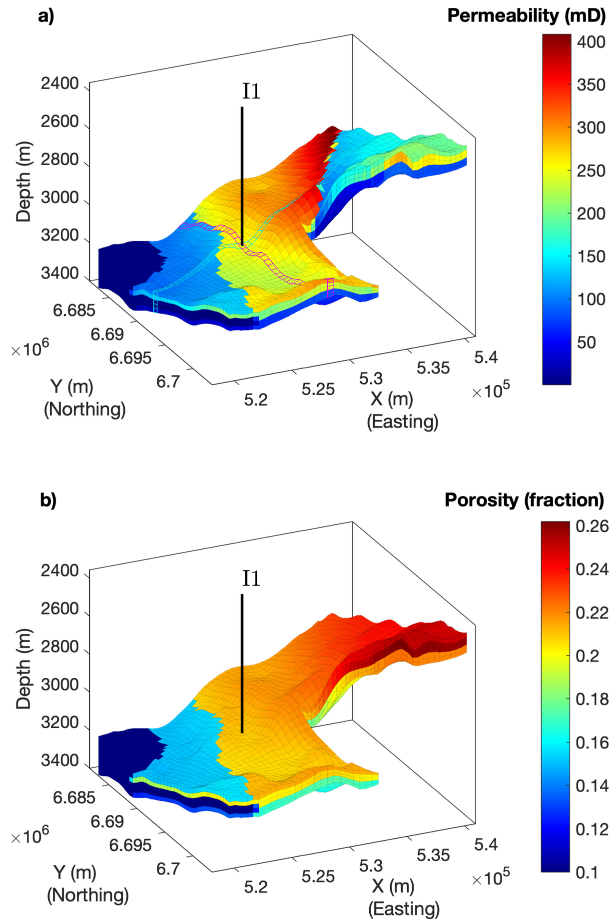

Fig. 2. True reservoir model of (a) permeability and (b) porosity of the deep saline aquifer in the Johansen formation. The coordinates are in the UTM system. The y-axis corresponds to the Northing direction, and the x-axis corresponds to the Easting direction. Black line: Location of the injector well.

based on the initial porosity model and the fluid saturations obtained from the simulator.

The synthetic time-lapse seismic data and CSEM data are generated using the geophysical forward models (4)–(11) and are shown in Figs. 3 and 4. The CSEM amplitudes are computed in the log10 domain [60] and the differences represent the variations in the logarithm of the amplitudes. Porosity is assumed to be constant in time; therefore, the differences in the geophysical data are due to the changes in saturation. We assume that the effect of pressure changes is negligible compared with the effect of saturation changes. The signal-to-noise ratio of the data is assumed to be 10. The data errors are assumed to be uncorrelated in time and space. Therefore, the covariance matrix of the measurements is diagonal.

B. Inversion Results

The inversion methodology is presented in two parts: first, we compute the porosity model based on the base seismic survey; then, we predict the CO_2 saturation based on the time-lapse seismic and CSEM data.

First, we estimate the porosity model from the base seismic survey using the Ensemble Smoother approach. We generate

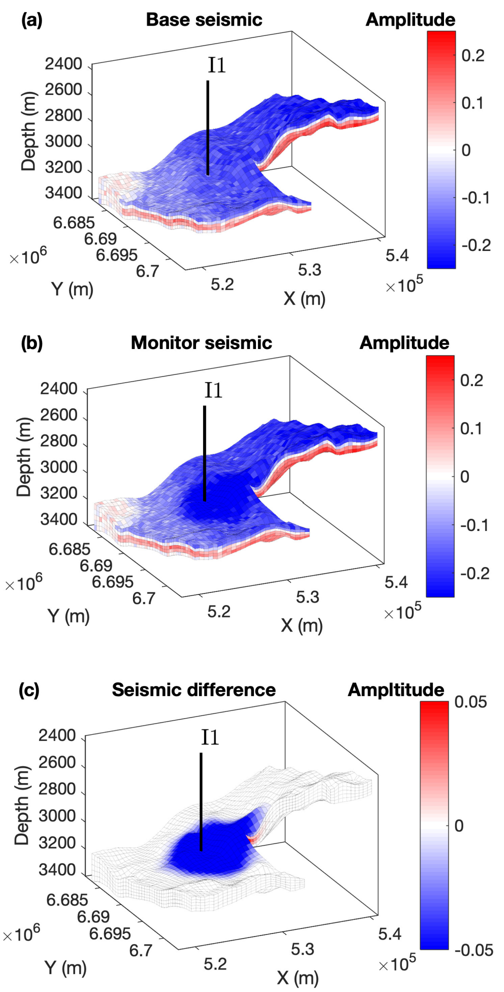

Fig. 3. Time-lapse seismic surveys. (a) Base seismic survey acquired before injection. (b) Monitor seismic survey. (c) Difference between base and monitor seismic data.

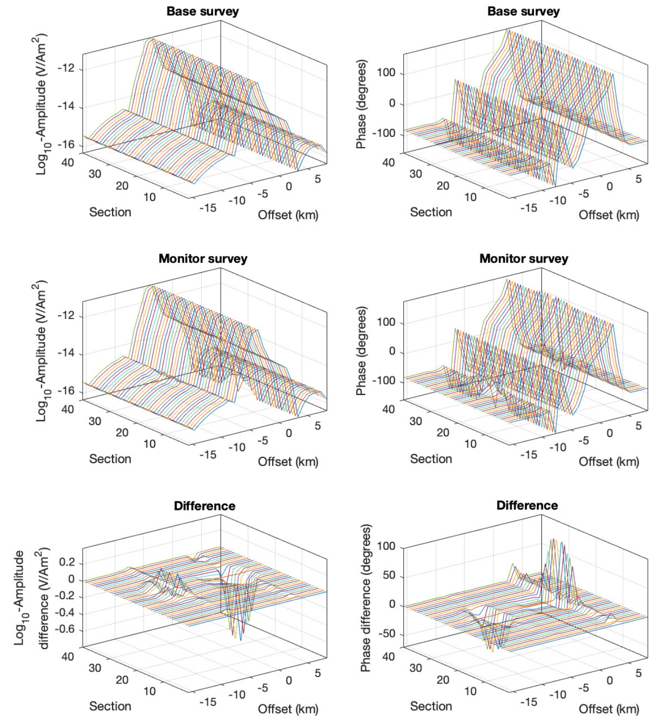

Fig. 4. Time-lapse CSEM surveys acquired before and after injection and their difference. (Left) Log-amplitude data. (Right) Phase. Each 2-D section is represented in a different color for clarity of illustration.

the initial ensemble of 100 prior realizations of porosity using the FFT-MA method. The models are generated by adding a locally variable prior mean to preserve the non-stationary trend of porosity in the vertical direction and the spatial anisotropic behavior. The mean of the 100 prior realizations of porosity in the top and bottom layers is shown in Fig. 5. Their seismic responses are generated using the rock physics model and the convolutional seismic model. Due to the large dimension of the data space, we re-parameterize the seismic data using sparse latent features by applying the DCAE and we perform inversion in the lower dimensional space. The posterior mean of the updated porosity models is shown in Fig. 5.

Then, we estimate the CO_2 saturation model in year 110, from monitor seismic and CSEM data. The 100 realizations in the initial ensemble of CO_2 saturation models are generated using dynamic simulations of CO_2 injection and geostatistical simulations of rock properties (permeability and porosity). For each of the geostatistical simulations of porosity and permeability, we simulate the fluid flow after injection using MRST-co2lab and select a saturation realization at a random time according to a uniform distribution on the simulation time interval. Using this approach for the generation of the initial ensemble, we preserve the hydrological realism of the saturation models in the prior and impose physical constraints that cannot be guaranteed by traditional geostatistical simulations. The mean of the CO_2 saturation prior realizations, in the top and bottom layers, is shown in Fig. 6.

The predicted seismic and CSEM responses of the prior realizations in year 110 are obtained by applying the seismic and electromagnetic forward models and using the predicted porosity model obtained in the first step of the inversion. A logit transformation is applied to the saturation models to perform inversion in the real number domain rather than the bounded saturation domain. A dimensionality reduction is applied to data before inversion. We then compute the posterior mean of the CO_2 saturation distribution conditioned on the monitor seismic and CSEM data, using the Ensemble Smoother. The posterior mean of the CO_2 saturation model is shown in Figs. 6 (map view) and 7 (vertical view of two orthogonal sections). The predicted model shows a good agreement with the true model. The standard deviation maps of porosity and CO_2 saturations are shown in Figs. 8 and 9, respectively, which show a reduction in the posterior standard deviation in both properties compared with the prior standard deviation of the initial ensemble.

A 3-D view of the CO_2 plume in year 110 is shown in Fig. 10. The prediction obtained through the geophysical inverse problem accurately matches the true model. To represent the posterior uncertainty in 3-D, we show the 0.90 confidence interval of the CO_2 saturation predictions. Fig. 11 shows the 5^{th} and 95^{th} percentile of the CO_2 saturation, that is, the lower and upper bounds of the 0.90 confidence interval. Overall, the pointwise confidence intervals are relatively

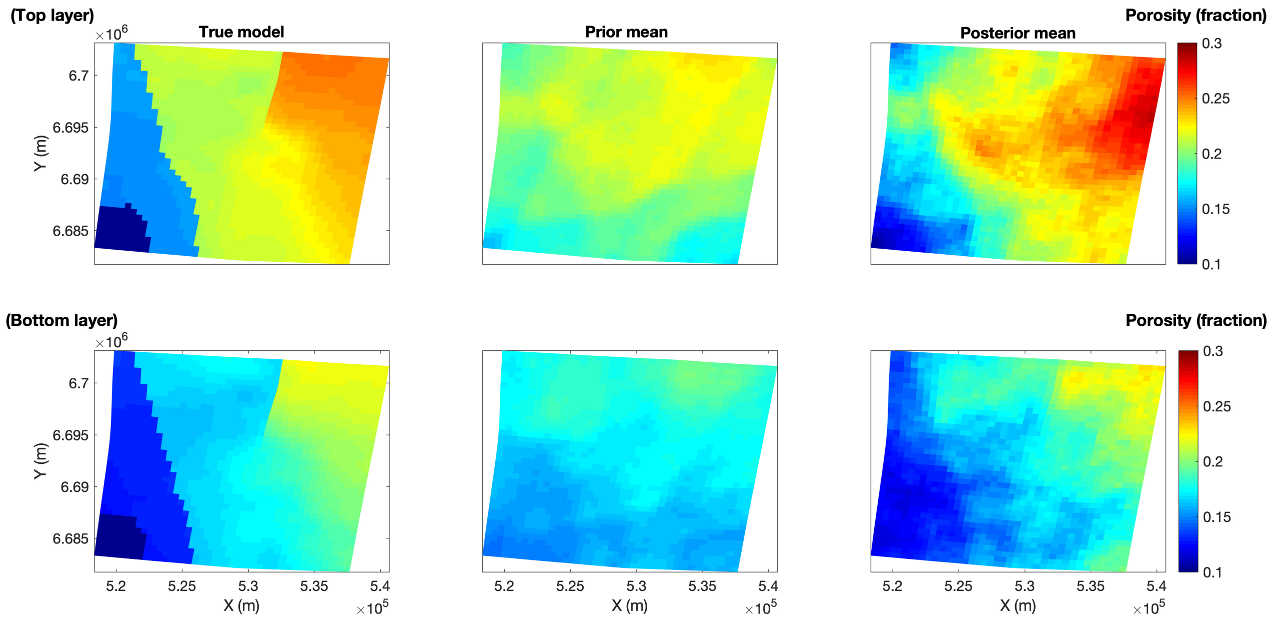

Fig. 5. Porosity model of the top reservoir layer (Top) and the bottom reservoir layer (Bottom). (From Left to Right) True model; prior mean; posterior mean predicted from seismic data.

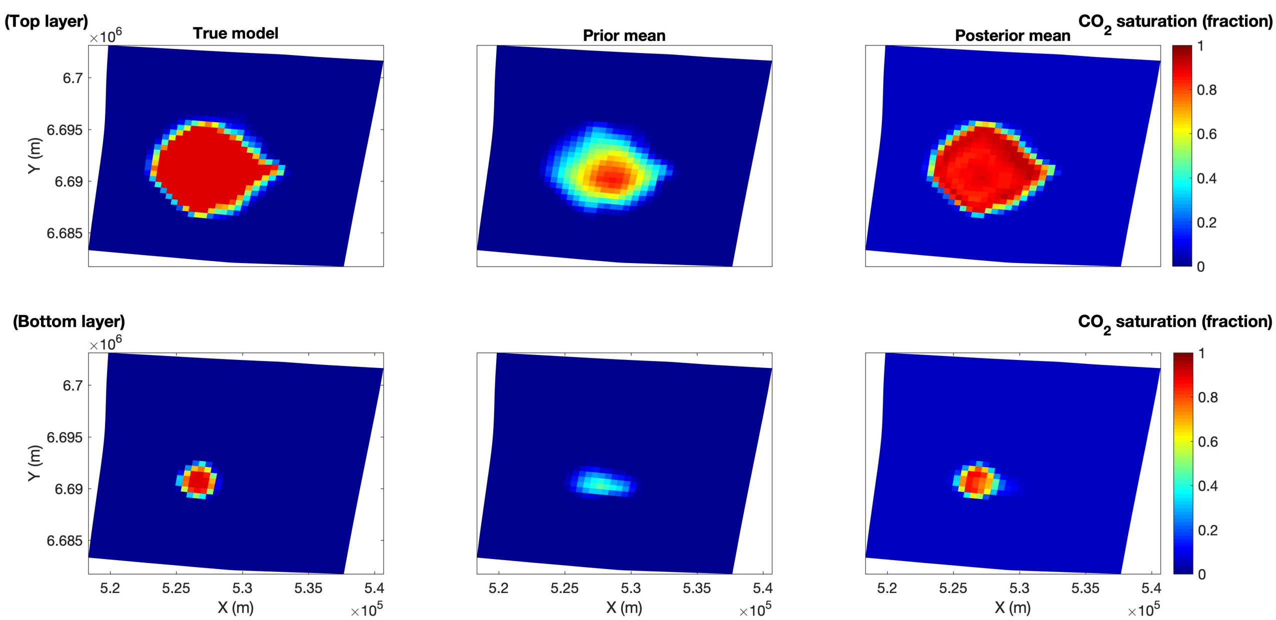

Fig. 6. CO_2 saturation model (map view) in year 110 of the top reservoir layer (Top) and the bottom reservoir layer (Bottom). (From Left to Right) True model; prior mean; posterior mean predicted from time-lapse geophysical data.

narrow, except close to the location near the CO_2 plume where the uncertainty is generally higher. The width of the confidence interval generally depends on the quality of the measured geophysical data and the approximations of the geophysical models. The correlation between the inversion prediction and the true saturation model is 0.96 in the entire model and 0.88 if we only consider the locations where saturation changes during the injection, which shows a high prediction accuracy. To evaluate uncertainty quantification, we computed the percentage of samples of true model within the 0.90 confidence interval, also known as the coverage ratio of the confidence interval, and estimated a value of 83%, which shows that uncertainty is slightly underestimated, possibly due to model linearization, limited ensemble size, and data reduction.

The proposed inversion results were compared with well-established inverse theory methods such as Occam's inversion and Bayesian linearized inversion which show a higher accuracy and a better reproduction of the spatial correlation structure of CO_2 saturation maps. The studied model is relatively small (8,000 grid cells), and therefore, a limited number of ensemble realizations can be used for stochastic inversion. For a larger model, it might be necessary to increase the number of model realizations in the initial ensemble to avoid the

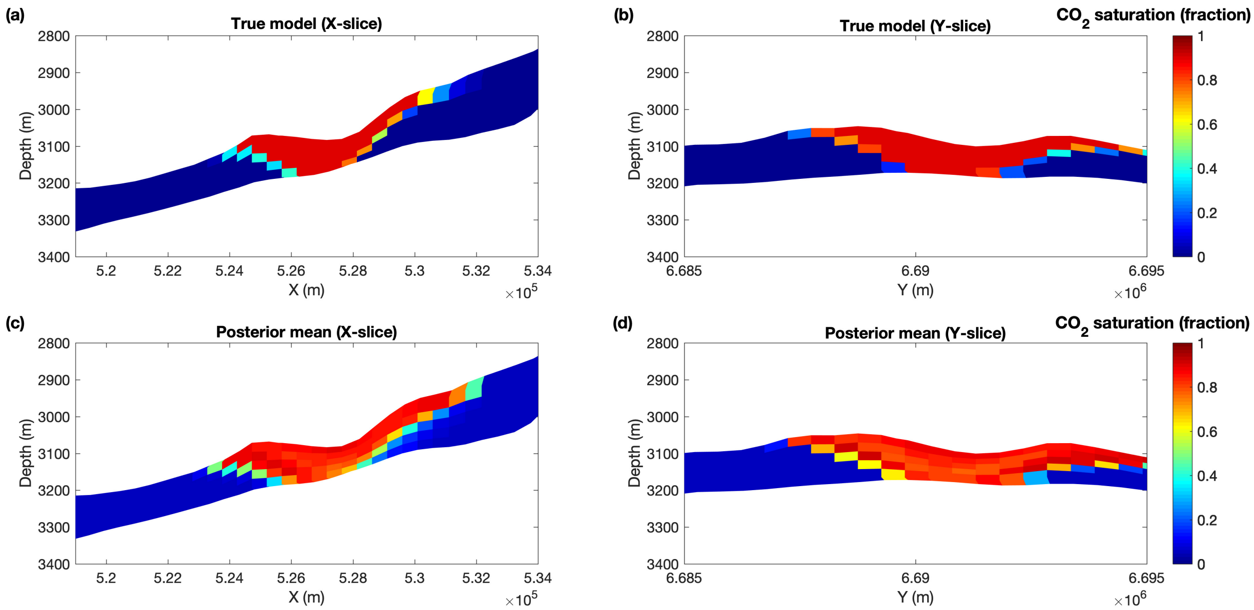

Fig. 7. CO_2 saturation model (section view) in year 110 of two orthogonal sections. (a) True model (X-slice). (b) True model (Y-slice). (c) Posterior mean (X-slice). (b) Posterior mean (Y-slice). The 3-D locations of the X- and Y-slices are shown in Fig. 2(a).

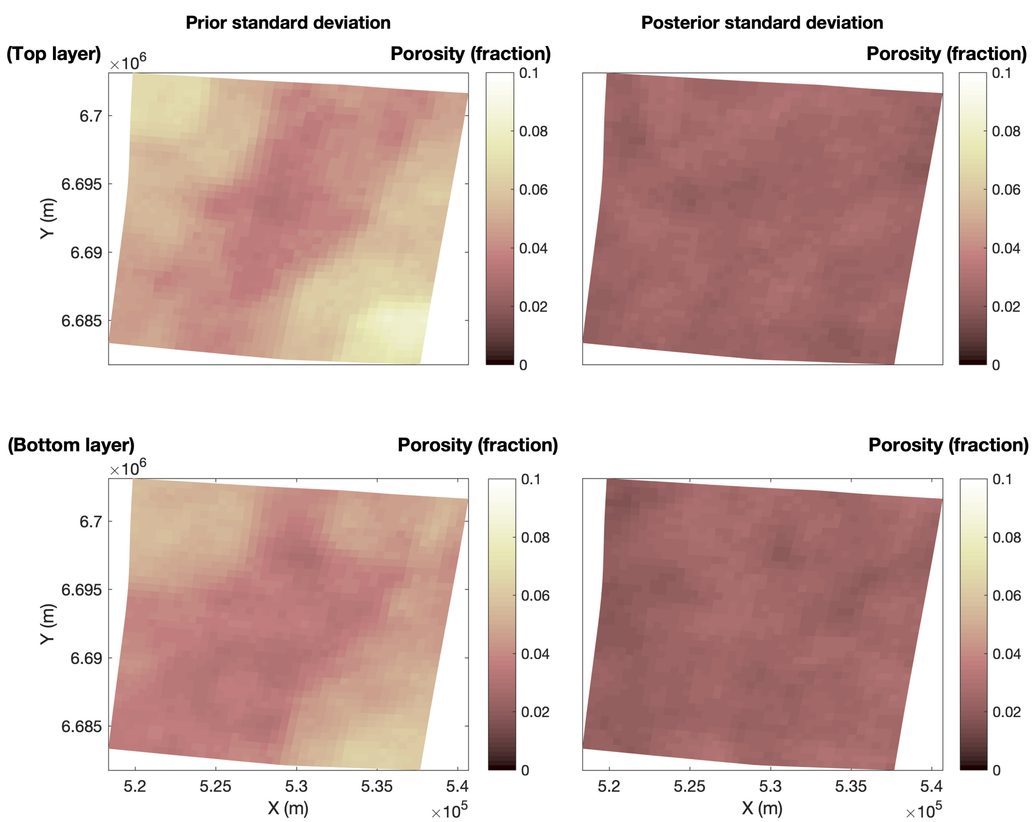

Fig. 8. Uncertainty quantification of the porosity model in the top and bottom layers. (Left) Prior standard deviation maps. (Right) Posterior standard deviation maps.

ensemble collapse. The results generally depend on the quality of the data, in terms of resolution and signal-to-noise ratio. In our application, we assumed a signal-to-noise ratio of 10; however, real data might show lower values and posterior uncertainty might be larger. The dimensionality reduction is generally necessary for 3-D data and the dimension of the reduced data space can be determined from the magnitude of the eigenvalues of the singular value decomposition of the data vector [49].

The impact of each data set, namely, seismic and CSEM surveys, has been investigated by performing the same inversion using only one of the two data sources. Using only seismic

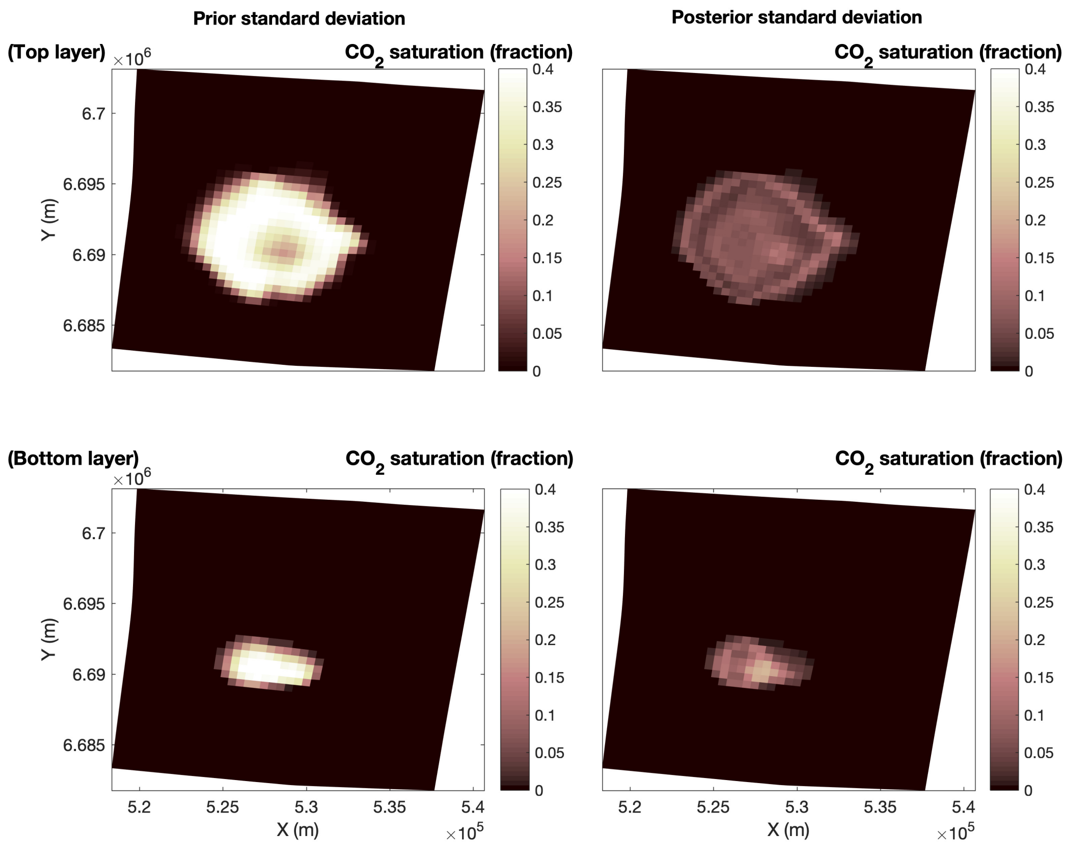

Fig. 9. Uncertainty quantification of the CO_2 saturation model in the top and bottom layers. (Left) Prior standard deviation maps. (Right) Posterior standard deviation maps.

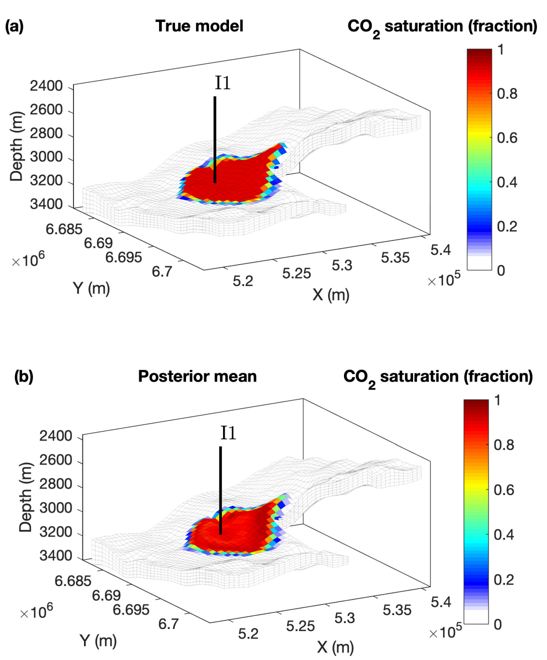

Fig. 10. CO_2 saturation model (3-D view) in year 110. (a) True model. (b) Posterior mean predicted from time-lapse geophysical data.

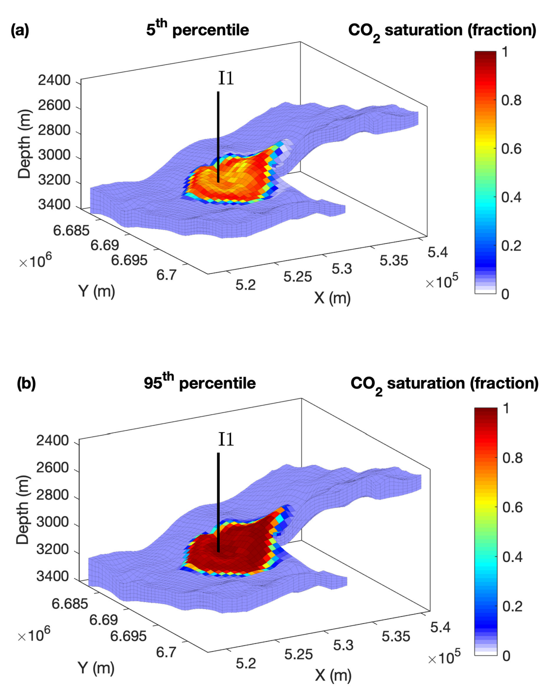

Fig. 11. Confidence interval 0.90 for the CO_2 saturation model in year 110. (a) 5^{th} percentile. (b) 95^{th} percentile.

data, inversion can accurately predict the location of the CO_2 plume but the results are less accurate in partially saturated rocks. This is due to the limited sensitivity of velocity to partial saturations and the large uncertainty of density estimation from seismic data. The correlation between predictions and true saturation model decreases to 0.79. Using only CSEM data, the accuracy of the predictions is strongly dependent on the frequency of the data, and the posterior standard deviation is overall larger than in the seismic case, due to data resolution. The correlation between predictions and true saturation model decreases to 0.77. Porosity and fluid saturations could be jointly inverted from base and monitor surveys; however, preliminary tests showed that the inversion results overestimate the correlation of the model variables and posterior uncertainty is underestimated.

The inversion code is written in MATLAB, whereas for forward models, we adopted different open source packages including the Fortran code MARE2DEM [53] and the MATLAB code MRST [55]. The computational cost for the inversion is approximately 3 h, with no parallelization, for the proposed model including 16 000 model variables (porosity and CO_2 saturation values at each reservoir location) and 14 800 measurements (base and monitor seismic and CSEM data) with 74% of the computational time spent on the forward geophysical model.

IV. Conclusion

We presented a stochastic inversion for the prediction of rock and fluid properties, namely, porosity and time-dependent CO_2 saturation values, from multiple source geophysical data, including seismic and electromagnetic surveys. The proposed Ensemble Smoother approach updates an ensemble of geostatically generated initial realizations in a Bayesian setting. The method was validated on synthetic time-lapse geophysical data generated for the Johansen formation model. The inversion results show high prediction accuracy and preserve a realistic spatial correlation structure for porosity and CO_2 saturation. This result is achieved by integrating geostatistical simulations to generate the initial porosity models and fluid flow simulations to generate the initial fluid saturation models. The initial realizations are updated conditioned on the mismatch between data predictions and measurements; therefore, the accuracy of the inversion depends on the signal-to-noise ratio and resolution of the data. The posterior standard deviation and confidence intervals provide a quantification of the uncertainty in predictions. The uncertainty in the proposed case study is relatively small due to the use of synthetic data; however, in real data studies, we can expect the saturation uncertainty to increase depending on the quality of the data. The proposed methodology was applied to a deep saline aquifer but could be extended to CO_2 sequestration studies in depleted hydrocarbon reservoirs as well as CO_2 injection and storage as part of EOR applications.

Acknowledgment

The authors would like to thank the School of Energy Resources, University of Wyoming and the Nielson Energy Fellowship, for the support. They would also like to thank Dr. K. Key (Lamont-Doherty Earth Observatory, Columbia University) for providing the code MARE2DEM and SINTEF for providing the package MATLAB Reservoir Simulation Toolbox (MRST). The data generated in this project and the inversion codes are available at the following link: https://tinyurl.com/yaq9y3on

References

[1] T. M. Davis, M. Landrø, and M. Wilson, *Geophysics and Geosequestration*. Cambridge, U.K.: Cambridge Univ. Press, 2019.
[2] P. Kitanidis, *Introduction to Geostatistics: Applications in Hydrogeology*. Cambridge, U.K.: Cambridge Univ. Press, 1997.
[3] D. Oliver, A. Reynolds, and N. Liu, *Inverse Theory for Petroleum Reservoir Characterization and History Matching*. Cambridge, U.K.: Cambridge Univ. Press, 2008.
[4] G. Mavko, T. Mukerji, and J. Dvorkin, *The Rock Physics Handbook*. Cambridge, U.K.: Cambridge Univ. Press, 2009.
[5] S. Bachu, "Review of CO_2 storage efficiency in deep saline aquifers," *Int. J. Greenhouse Gas Control*, vol. 40, pp. 188–202, Sep. 2015.
[6] A. Goodman, S. Sanguinito, and J. S. Levine, "Prospective CO_2 saline resource estimation methodology: Refinement of existing US-DOE-NETL methods based on data availability," *Int. J. Greenhouse Gas Control*, vol. 54, pp. 242–249, Nov. 2016.
[7] S. E. Gasda, H. M. Nilsen, H. K. Dahle, and W. G. Gray, "Effective models for CO_2 migration in geological systems with varying topography," *Water Resour. Res.*, vol. 48, no. 10, pp. 1–17, Oct. 2012.
[8] M. L. Szulczewski, C. W. Macminn, H. J. Herzog, and R. Juanes, "Lifetime of carbon capture and storage as a climate-change mitigation technology," *Proc. Nat. Acad. Sci. USA*, vol. 109, no. 14, pp. 5185–5189, Apr. 2012.
[9] J. M. Nordbotten *et al.*, "Uncertainties in practical simulation of CO_2 storage," *Int. J. Greenhouse Gas Control*, vol. 9, pp. 234–242, Jul. 2012.
[10] C. D. Gorecki, S. C. Ayash, J. R. Braunberger, N. W. Dotzenrod, and G. Liu, "A comparison of volumetric and dynamic CO_2 storage resource and efficiency in deep saline formations," *Int. J. Greenhouse Gas Control*, vol. 42, pp. 213–225, Nov. 2015.
[11] B. Li and S. M. Benson, "Influence of small-scale heterogeneity on upward CO_2 plume migration in storage aquifers," *Adv. Water Resour.*, vol. 83, pp. 389–404, Sep. 2015.
[12] H. Büsing, C. Vogt, A. Ebigbo, and N. Klitzsch, "Numerical study on CO_2 leakage detection using electrical streaming potential data," *Water Resour. Res.*, vol. 53, no. 1, pp. 455–469, Jan. 2017.
[13] A. Chadwick, R. Arts, O. Eiken, P. Williamson, and G. Williams, "Geophysical monitoring of the CO_2 plume at Sleipner, North Sea," in *Advances in the Geological Storage of Carbon Dioxide*. Dordrecht, The Netherlands: Springer, 2006, pp. 303–314.
[14] G. T. Eigestad, H. K. Dahle, B. Hellevang, F. Riis, W. T. Johansen, and E. Øian, "Geological modeling and simulation of CO_2 injection in the Johansen formation," *Comput. Geosci.*, vol. 13, no. 4, p. 435, 2009.
[15] P. E. S. Bergmo, A.-A. Grimstad, and E. Lindeberg, "Simultaneous CO_2 injection and water production to optimise aquifer storage capacity," *Int. J. Greenhouse Gas Control*, vol. 5, no. 3, pp. 555–564, May 2011.
[16] S. Grude, M. Landrø, and B. Osdal, "Time-lapse pressure–saturation discrimination for CO_2 storage at the Snøhvit field," *Int. J. Greenhouse Gas Control*, vol. 19, pp. 369–378, Nov. 2013.
[17] D. Grana *et al.*, "A rock physics and seismic reservoir characterization study of the rock springs uplift, a carbon dioxide sequestration site in Southwestern Wyoming," *Int. J. Greenhouse Gas Control*, vol. 63, pp. 296–309, Aug. 2017.
[18] L. A. N. Roach and D. J. White, "Evolution of a deep CO_2 plume from time-lapse seismic imaging at the Aquistore storage site, Saskatchewan, Canada," *Int. J. Greenhouse Gas Control*, vol. 74, pp. 79–86, Jul. 2018.
[19] Z. Wang, W. P. Harbert, R. M. Dilmore, and L. Huang, "Modeling of time-lapse seismic monitoring using CO_2 leakage simulations for a model CO_2 storage site with realistic geology: Application in assessment of early leak-detection capabilities," *Int. J. Greenhouse Gas Control*, vol. 76, pp. 39–52, Sep. 2018.
[20] S. Glubokovskikh *et al.*, "How well can time-lapse seismic characterize a small CO_2 leakage into a saline aquifer: CO2CRC Otway 2C experiment (Victoria, Australia)," *Int. J. Greenhouse Gas Control*, vol. 92, Jan. 2020, Art. no. 102854.
[21] G. M. Hoversten *et al.*, "Direct reservoir parameter estimation using joint inversion of marine seismic AVA and CSEM data," *Geophysics*, vol. 71, no. 3, pp. C1–C13, May 2006.
[22] J. Chen, G. M. Hoversten, D. Vasco, Y. Rubin, and Z. Hou, "A Bayesian model for gas saturation estimation using marine seismic AVA and CSEM data," *Geophysics*, vol. 72, no. 2, pp. WA85–WA95, Mar. 2007.
[23] M. Lien and T. Mannseth, "Sensitivity study of marine CSEM data for reservoir production monitoring," *Geophysics*, vol. 73, no. 4, pp. F151–F163, Jul. 2008.
[24] A. Orange, K. Key, and S. Constable, "The feasibility of reservoir monitoring using time-lapse marine CSEM," *Geophysics*, vol. 74, no. 2, pp. F21–F29, Mar. 2009.

[25] K. Key and J. Ovall, "A parallel goal-oriented adaptive finite element method for 2.5-D electromagnetic modelling," *Geophys. J. Int.*, vol. 186, no. 1, pp. 137–154, Jul. 2011.
[26] A. H. Bhuyian, M. Landrø, and S. E. Johansen, "3D CSEM modeling and time-lapse sensitivity analysis for subsurface CO_2 storage," *Geophysics*, vol. 77, no. 5, pp. E343–E355, Sep. 2012.
[27] L. MacGregor, "Integrating seismic, CSEM, and well-log data for reservoir characterization," *Lead. Edge*, vol. 31, no. 3, pp. 268–277, 2012.
[28] E. Gasperikova and G. M. Hoversten, "A feasibility study of nonseismic geophysical methods for monitoring geologic CO_2 sequestration," *Lead. Edge*, vol. 25, no. 10, pp. 1282–1288, Oct. 2006.
[29] M. Commer, J. Doetsch, B. Dafflon, Y. Wu, T. M. Daley, and S. S. Hubbard, "Time-lapse 3-D electrical resistance tomography inversion for crosswell monitoring of dissolved and supercritical CO_2 flow at two field sites: Escatawpa and Cranfield, Mississippi, USA," *Int. J. Greenhouse Gas Control*, vol. 49, pp. 297–311, Jun. 2016.
[30] Y. Hu, R.-S. Wu, L.-G. Han, and P. Zhang, "Joint multiscale direct envelope inversion of phase and amplitude in the time–frequency domain," *IEEE Trans. Geosci. Remote Sens.*, vol. 57, no. 7, pp. 5108–5120, Jul. 2019.
[31] J. B. Rittgers, A. Revil, M. A. Mooney, M. Karaoulis, L. Wodajo, and C. J. Hickey, "Time-lapse joint inversion of geophysical data with automatic joint constraints and dynamic attributes," *Geophys. J. Int.*, vol. 207, no. 3, pp. 1401–1419, Dec. 2016.
[32] T. Lan, H. Liu, N. Liu, J. Li, F. Han, and Q. H. Liu, "Joint inversion of electromagnetic and seismic data based on structural constraints using variational born iteration method," *IEEE Trans. Geosci. Remote Sens.*, vol. 56, no. 1, pp. 436–445, Jan. 2018.
[33] T. Lan, N. Liu, F. Han, and Q. H. Liu, "Joint petrophysical and structural inversion of electromagnetic and seismic data based on volume integral equation method," *IEEE Trans. Geosci. Remote Sens.*, vol. 57, no. 4, pp. 2075–2086, Apr. 2019.
[34] D. Colombo and D. Rovetta, "Coupling strategies in multiparameter geophysical joint inversion," *Geophys. J. Int.*, vol. 215, no. 2, pp. 1171–1184, Nov. 2018.
[35] J. Sun and Y. Li, "Joint inversion of multiple geophysical and petrophysical data using generalized fuzzy clustering algorithms," *Geophys. J. Int.*, vol. 208, no. 2, pp. 1201–1216, Feb. 2017.
[36] J. Giraud, V. Ogarko, M. Lindsay, E. Pakyuz-Charrier, M. Jessell, and R. Martin, "Sensitivity of constrained joint inversions to geological and petrophysical input data uncertainties with posterior geological analysis," *Geophys. J. Int.*, vol. 218, no. 1, pp. 666–688, Jul. 2019.
[37] G. Li, H. Cai, and C.-F. Li, "Alternating joint inversion of controlled-source electromagnetic and seismic data using the joint total variation constraint," *IEEE Trans. Geosci. Remote Sens.*, vol. 57, no. 8, pp. 5914–5922, Aug. 2019.
[38] R. Tavakoli, H. Yoon, M. Delshad, A. H. ElSheikh, M. F. Wheeler, and B. W. Arnold, "Comparison of ensemble filtering algorithms and null-space Monte Carlo for parameter estimation and uncertainty quantification using CO_2 sequestration data," *Water Resour. Res.*, vol. 49, no. 12, pp. 8108–8127, Dec. 2013.
[39] Y. Sun, C. Tong, W. J. Trainor-Guitton, C. Lu, K. Mansoor, and S. A. Carroll, "Global sampling for integrating physics-specific subsystems and quantifying uncertainties of CO_2 geological sequestration," *Int. J. Greenhouse Gas Control*, vol. 12, pp. 108–123, Jan. 2013.
[40] G. Evensen and P. J. van Leeuwen, "An ensemble Kalman smoother for nonlinear dynamics," *Monthly Weather Rev.*, vol. 128, no. 6, pp. 1852–1867, Jun. 2000.
[41] G. Evensen, *Data Assimilation: The Ensemble Kalman Filter*. Berlin, Germany: Springer, 2009.
[42] Y. Chen and D. S. Oliver, "Ensemble randomized maximum likelihood method as an iterative ensemble smoother," *Math. Geosci.*, vol. 44, no. 1, pp. 1–26, Jan. 2012.
[43] A. A. Emerick and A. C. Reynolds, "Ensemble smoother with multiple data assimilation," *Comput. Geosci.*, vol. 55, pp. 3–15, Jun. 2013.
[44] A. A. Emerick, "Estimation of pressure and saturation fields from time-lapse impedance data using the ensemble smoother," *J. Geophys. Eng.*, vol. 11, no. 3, Jun. 2014, Art. no. 035007.
[45] H. Ghorbanidehno, A. Kokkinaki, J. Y. Li, E. Darve, and P. K. Kitanidis, "Real-time data assimilation for large-scale systems: The spectral Kalman filter," *Adv. Water Resour.*, vol. 86, pp. 260–272, Dec. 2015.
[46] S. Tveit, S. A. Bakr, M. Lien, and T. Mannseth, "Ensemble-based Bayesian inversion of CSEM data for subsurface structure identification," *Geophys. J. Int.*, vol. 201, no. 3, pp. 1849–1867, Jun. 2015.
[47] W. Ma, B. Jafarpour, and J. Qin, "Dynamic characterization of geologic CO_2 storage aquifers from monitoring data with ensemble Kalman filter," *Int. J. Greenhouse Gas Control*, vol. 81, pp. 199–215, Feb. 2019.
[48] C. Bobe, E. Van De Vijver, J. Keller, D. Hanssens, M. Van Meirvenne, and P. De Smedt, "Probabilistic 1-D inversion of frequency-domain electromagnetic data using a Kalman ensemble generator," *IEEE Trans. Geosci. Remote Sens.*, vol. 58, no. 5, pp. 3287–3297, May 2020.
[49] M. Liu and D. Grana, "Stochastic nonlinear inversion of seismic data for the estimation of petroelastic properties using the ensemble smoother and data reparameterization," *Geophysics*, vol. 83, no. 3, pp. M25–M39, May 2018.
[50] S. Tveit, T. Mannseth, J. Park, G. Sauvin, and R. Agersborg, "Combining CSEM or gravity inversion with seismic AVO inversion, with application to monitoring of large-scale CO_2 injection," *Comput. Geosci.*, vol. 24, pp. 1201–1220, Mar. 2020.
[51] A. Tarantola, *Inverse Problem Theory and Methods for Model Parameter Estimation*. Philadelphia, PA, USA: SIAM, 2005.
[52] K. Aki and P. G. Richards, *Quantitative Seismology*. Mill Valley, CA, USA: University Science Books, 2002.
[53] K. Key, "MARE2DEM: A 2-D inversion code for controlled-source electromagnetic and magnetotelluric data," *Geophys. J. Int.*, vol. 207, no. 1, pp. 571–588, Oct. 2016.
[54] M. Le Ravalec, B. Noetinger, and L. Y. Hu, "The FFT moving average (FFT-MA) generator: An efficient numerical method for generating and conditioning Gaussian simulations," *Math. Geol.*, vol. 32, no. 6, pp. 701–723, 2000.
[55] K. Lie, *An Introduction to Reservoir Simulation Using MATLAB/GNU Octave*. Cambridge, U.K.: Cambridge Univ. Press, 2019.
[56] W. Nowak, "Best unbiased ensemble linearization and the quasi-linear Kalman ensemble generator," *Water Resour. Res.*, vol. 45, no. 4, Apr. 2009.
[57] M. Liu and D. Grana, "Time-lapse seismic history matching with an iterative ensemble smoother and deep convolutional autoencoder," *Geophysics*, vol. 85, no. 1, pp. M15–M31, Jan. 2020.
[58] Z. Gao, Z. Pan, C. Zuo, J. Gao, and Z. Xu, "An optimized deep network representation of multimutation differential evolution and its application in seismic inversion," *IEEE Trans. Geosci. Remote Sens.*, vol. 57, no. 7, pp. 4720–4734, Jul. 2019.
[59] S. Li *et al.*, "Deep-learning inversion of seismic data," *IEEE Trans. Geosci. Remote Sens.*, vol. 58, no. 3, pp. 2135–2149, Mar. 2020.
[60] B. Wheelock, S. Constable, and K. Key, "The advantages of logarithmically scaled data for electromagnetic inversion," *Geophys. J. Int.*, vol. 201, no. 3, pp. 1765–1780, Jun. 2015.

Dario Grana received the Ph.D. degree in geophysics from Stanford University, Stanford, CA, USA, in 2013.

He is an Associate Professor with the Department of Geology and Geophysics, University of Wyoming. He is the coauthor of *Seismic Reflections of Rock Properties* (Cambridge University Press, 2014). His main research interests are rock physics, seismic reservoir characterization, geostatistics, data assimilation, and inverse problems for subsurface modeling.

Dr. Grana is the recipient of the 2017 EAGE Van Weelden Award and the 2016 SEG Karcher Award.

Mingliang Liu received the M.Sc. degree in petroleum geology from the China University of Geosciences, Wuhan, China, in 2016. He is pursuing the Ph.D. degree with the Department of Geology and Geophysics, University of Wyoming, Laramie, WY, USA.

He is the first author of four publications on stochastic methods for seismic inversion and reservoir characterization. His areas of expertise are petroelastic inversion, rock physics, and machine learning.

Mohit Ayani received the M.Sc. degree in applied geophysics from the Indian School of Mines, in 2015. He is pursuing the Ph.D. degree with the Department of Geology and Geophysics, University of Wyoming.

He is the first author of two publications on stochastic methods for electromagnetic inversion and time-lapse studies. His areas of expertise are CSEM inversion, rock physics, and parallel computing.